Conference "Nonlinearity, Bifurcation, Chaos: the Doors to the Future", Poland, 16-18 Sept. 1996

# 3-D CHAOS IN THE THIN ELASTIC ROD

E.L. Starostin

Keldysh Institute of Applied Mathematics, Russian Academy of Sciences,

Miusskaya Sq. 4, 125047 Moscow, Russia

*Abstract:* Equilibrium shapes of a thin homogeneous elastic rod are considered. It is assumed that the rod is straight and twisted in its relaxed state and it is submitted to external forces at its ends only. The torsional stiffness and two principal bending stiffnesses are assumed to be constant and all different. The initial twisting rate is also taken to be constant along the rod. These assumptions turn out to be sufficient to produce chaotic 3-D shapes of the rod. The phase space of the system under consideration is investigated by reducing it to a mapping of two-dimensional Poincaré sections. The results obtained are illustrated graphically.

## 1. Introduction

Equilibrium shapes of a thin homogeneous elastic rod obey equations identical to those governing the rotation of a gyrostat spinning about a fixed point in a constant homogeneous gravitational field (the Kirchhoff analogy). The equations are integrable when the rod has a circular cross section and its bending stiffness coefficients are equal. This model has been widely used for investigation of shapes of a DNA molecule, e. g., see [Šelepová & Kypr, 1985]. Equilibrium configurations of the axisymmetric rod closed into a ring were studied in [Starostin, 1996].

On the other hand, the problems of spatial chaos were considered in [Davies & Moon, 1993] for an infinitely long elastic rod for two cases: when one of bending stiffness coefficients or initial curvatures changes periodically along the rod while all other stiffnesses and initial curvatures are constant.

In this paper, the torsional stiffness and two principal bending stiffnesses are assumed to be constant and different. The initial twisting rate is also taken to be constant along the rod. These assumptions turn out to be sufficient to produce chaotic 3-D shapes of the rod. It should be noted that chaos is treated here in the limiting sense [El Naschie & Kapitaniak, 1990].

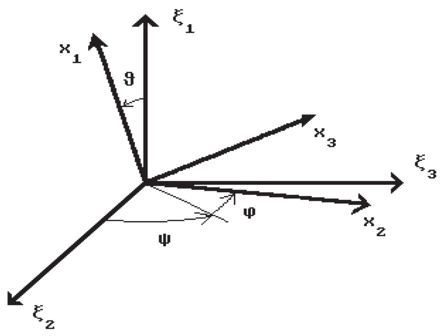


Figure 1: The Euler angles $\psi$, $\varphi$, and $\vartheta$ specify the attitude of the principal axes of bending and twisting $x_1x_2x_3$ with respect to the coordinate system $\xi_1\xi_2\xi_3$ fixed in space. The axis $x_1$ is along the center line of the rod. The direction of the axis $\xi_1$ is coincident with the direction of the end force.

The phase space of the system under consideration may be investigated by reducing it to a mapping of two-dimensional Poincaré sections. The Poincaré maps were built numerically for various values of parameters of the rod. Different choice of Poincaré sections was tried in order to obtain thorough data on the whole phase space structure. The maximum Lyapunov exponents were computed to identify chaotic trajectories and to characterize the level of chaoticity. The results obtained are illustrated graphically.

**2. Equations**

We consider an initially curved and/or twisted thin elastic rod which is deformed by the forces and moments at its ends only. Its equilibrium state is described by the following system of differential equations [Ilyukhin, 1979]:

$$\begin{aligned} b\frac{d\omega_1}{ds} + c\omega_2(\omega_3 - \omega_3^0) - \omega_3(\omega_2 - \omega_2^0) = 0, \\ \frac{d\omega_2}{ds} + b\omega_3(\omega_1 - \omega_1^0) - c\omega_1(\omega_3 - \omega_3^0) - \frac{p}{2}\sin\vartheta\cos\varphi = 0, \\ c\frac{d\omega_3}{ds} - b\omega_2(\omega_1 - \omega_1^0) + \omega_1(\omega_2 - \omega_2^0) + \frac{p}{2}\sin\vartheta\sin\varphi = 0, \end{aligned} \tag{1}$$

where $\omega_1$ is the torsion of the cross section about the tangent to the center line of the rod, $\omega_2$ and $\omega_3$ are projections of the curvature of the center line onto the principal axes of bending, $s$ the arc coordinate along the center line, which extension is neglected, $\omega_1^0$ an initial value of the torsion in the relaxed state, $\omega_2^0$ and $\omega_3^0$ initial values of the curvature projections in the relaxed state, $b = B_{11}/B_{22}, c = B_{33}/B_{22} (B_{22} \neq 0), B_{11}$ the torsional stiffness coefficient, $B_{22}$ and $B_{33}$ the principal bending stiffness coefficients, $p = -2P/B_{22}, P$ the value of the end force.

The attitude of the principal axes of bending and twisting $x_1x_2x_3$ with respect to the fixed coordinate system $\xi_1\xi_2\xi_3$ is given by the three Euler angles $\psi, \varphi, \vartheta$ (Fig. 1). The axis $\xi_1$ is aligned with the direction of the end force.

The vector $\vec{\omega} = (\omega_1, \omega_2, \omega_3)$ specifies the angular velocity of rotation of the axes $x_1x_2x_3$ with respect to the fixed coordinate system. An analog of the Euler kinematic equations

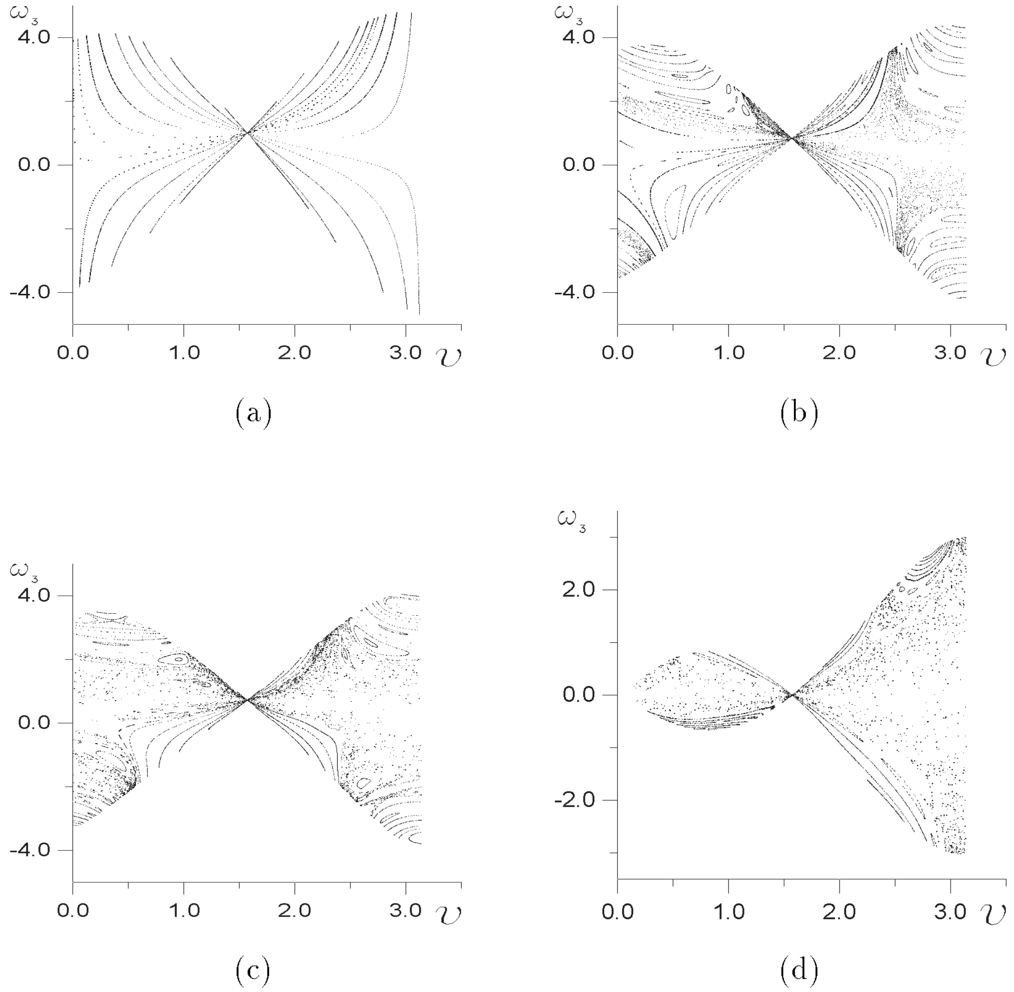


Figure 2: Poincaré maps of $(\vartheta, \omega_3)$ plane. (a) $B_{11}/B_{22} = 0.8, B_{33}/B_{22} = 1.0, p = 3., l = 1., e = 20., \omega_1^0 = 0.2$. A symmetric rod, an integrable case. (b) $B_{11}/B_{22} = 0.8, B_{33}/B_{22} = 1.2, p = 3., l = 1., e = 20., \omega_1^0 = 0.2$. (c) $B_{11}/B_{22} = 0.8, B_{33}/B_{22} = 1.4, p = 3., l = 1., e = 20., \omega_1^0 = 0.2$. (d) $B_{11}/B_{22} = 0.8, B_{33}/B_{22} = 1.1, p = 5., l = 0., e = 5., \omega_1^0 = 0.2$.

is valid

$$\frac{d\psi}{ds} = \frac{\omega_2 \sin\varphi + \omega_3 \cos\varphi}{\sin\vartheta}, \qquad (2)$$

$$\frac{d\varphi}{ds} = \omega_1 - \cot\vartheta(\omega_2 \sin\varphi + \omega_3 \cos\varphi),$$

$$\frac{d\vartheta}{ds} = \omega_2 \cos\varphi - \omega_3 \sin\varphi.$$

The system of Eqs. (1),(2) allows for the invariants

$$b(\omega_1 - \omega_1^0)\cos\vartheta + (\omega_2 - \omega_2^0)\sin\vartheta\sin\varphi + c(\omega_3 - \omega_3^0)\sin\vartheta\cos\varphi = l, \qquad (3)$$

$$b\omega_1^2 + \omega_2^2 + c\omega_3^2 + p\cos\vartheta = e, \qquad (4)$$

## 3. The Poincaré Mapping

In what follows, we assume that the rod is straight in the relaxed state, then $\omega_2^0 = \omega_3^0 = 0$. However, the rod may be twisted (generally, $\omega_1^0 \neq 0$). This case corresponds to the model of DNA [Šelepová & Kypr, 1985], [Starostin, 1996].

The system (1), (2) is not integrable in the general case. Note that the variable $\psi$ does not appear in the right sides of Eqs. (1), (2) and the first Eq. (2) may be solved after the solution of the rest 5 equations. Since the variable $\varphi$ appears in the right sides as an argument of trigonometric functions, we may study the system's configurations only at the time moments when $\varphi = 2\pi k, k$ integer. The configuration is completely described by the values of $\omega_1, \omega_2, \omega_3$ and $\vartheta$, which satisfy (3) and (4). $\omega_1$ may be eliminated from (3) and (4) and we obtain one equation that constrains the values of $\omega_2, \omega_3$ and $\vartheta$:

$$b\left(\omega_1^0 + \frac{l - c\omega_3 \sin\vartheta}{b\cos\vartheta}\right)^2 + \omega_2^2 + c\omega_3^2 + p\cos\vartheta = e. \tag{5}$$

For a fixed $\vartheta$, Eq. (5) defines a second-order curve on the plane $(\omega_2, \omega_3)$. It is easy to show that this curve may be only an ellipse (real or imaginary) or a pair of imaginary straight lines having a common real point. The second case always takes place when $\vartheta = \frac{\pi}{2} : \omega_2 = 0, \omega_3 = \frac{l}{c}$.

We will consider such values of parameters when a real ellipse exists at least for some interval(s) of $\vartheta$. Then there is a surface in the space $(\omega_2, \omega_3, \vartheta)$. We choose this surface as a surface of section and we compute the Poincaré maps of it. Numerical integration is applied to obtain the Poincaré maps.

## 4. Numerical Results

The Poincaré maps are presented as projections on $(\vartheta, \omega_3)$ plane in Fig. 2. The maps (a)–(c) are computed for the following values of the parameters: $b = B_{11}/B_{22} = 0.8, p = 3., l = 1., e = 20.$, and $\omega_1^0 = 0.2$. The parameter $c = B_{33}/B_{22}$ was taken different: (a) $c = 1.0$, (b) $c = 1.2$, (c) $c = 1.4$. The graph (a) corresponds to the symmetric rod. This case is integrable and one can see no chaotic trajectories on the map. To the contrary, there are chaotic regions on maps (b) and (c). The more the rod differs from symmetric, the more chaotic the map appears. Also, a complex structure of the phase space can be observed in Fig. 2 (b). There exist all kinds of solutions: periodic, quasiperiodic and chaotic.

The map (d) is presented for a lower energy level $e = 5.$ and for different $p = 5.$ and $l = 0.$ The rod is close to symmetrical: $c = 1.1$. However, there is a strong chaoticity of the map along with some islands of regular solutions. Further decrease in the energy implies an increase of the chaotic region. There exist such values of the parameters when no regular solutions were found.

## 5. Concluding Remarks

The results obtained may help in better understanding complexity of spatial configurations formed by long biopolymer molecules: DNAs, RNAs and proteins. In nature and technics, there are also many other long coiled structures which demonstrate similar properties and whose essential features may be approximately described by the same equations.

## Acknowledgements

This research is supported by the Russian Foundation of Basic Research Grant No. 95-01-00308 and by INTAS Grant No. 94-0643.

**References**


Davies, M.A. & Moon, F.C. [1993] "3-D spatial chaos in the elastica and the spinning top: Kirchhoff analogy", *Chaos* **3(1)**, 93–99.

El Naschie, M.S. & Kapitaniak, T. [1990] "Soliton chaos models for mechanical and biological elastic chains", *Physics Letters A* **147(5, 6)** 275–281.

Ilyukhin, A.A. [1979] *Spatial Problems of the Nonlinear Theory of Elastic Rods* (Naukova Dumka, Kiev) Chap. 1, pp. 7–34 [in Russian].

Šelepová, P. & Kypr, J. [1985] "Computer simulation of DNA supercoiling in a simple elastomechanical approximation", *Biopolymers* **24**, 867–882.

Starostin, E.L. [1996] "Three-dimensional conformations of looped DNA", *Meccanica* **31(3)**, 235–271.

# Appendix: Additional figures for transparencies

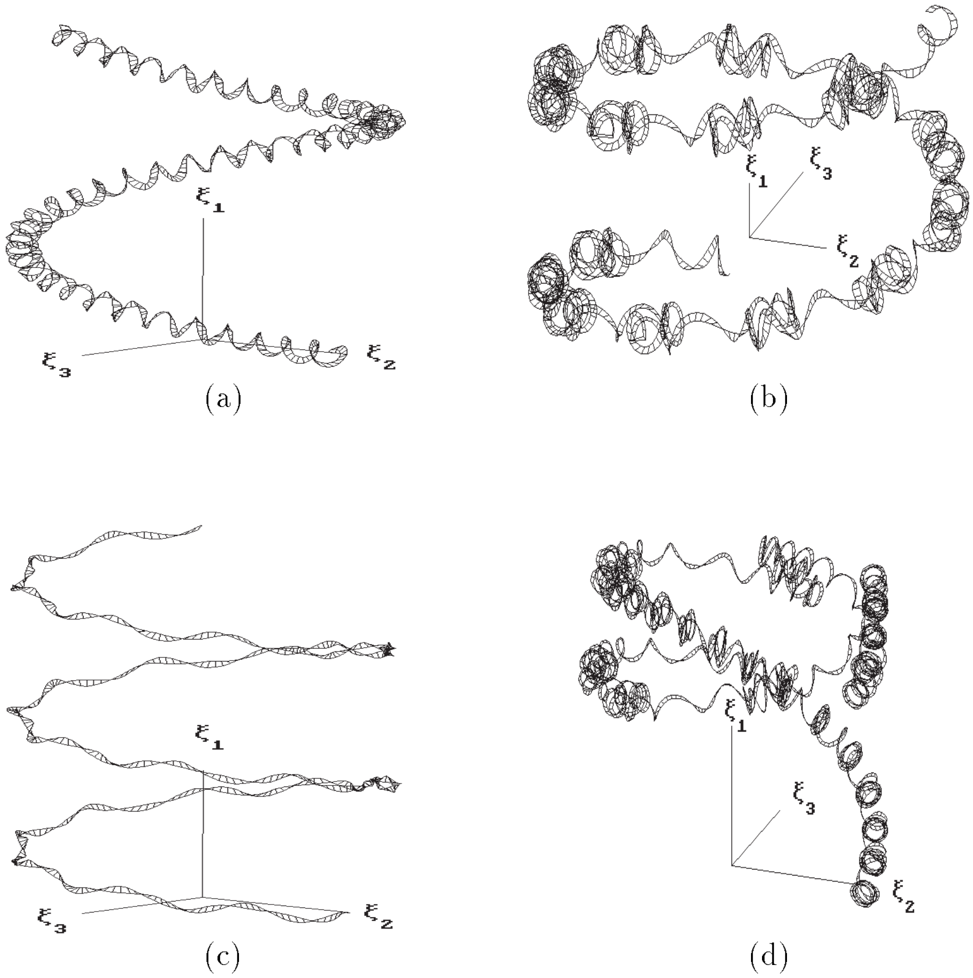


Figure 3: The shape of the rod in space.

(a) $B_{11}/B_{22} = 0.8, B_{33}/B_{22} = 1.0, p = 3., l = 1., e = 20., \omega_1^0 = 0.2,$
$\vartheta_0 = 0.4189, \omega_{30} = -1.017$. A symmetric rod, an integrable case.
(b) $B_{11}/B_{22} = 0.8, B_{33}/B_{22} = 1.2, p = 3., l = 1., e = 20., \omega_1^0 = 0.2.$
$\vartheta_0 = 0.6283, \omega_{30} = 1.698.$
(c) $B_{11}/B_{22} = 0.8, B_{33}/B_{22} = 1.2, p = 3., l = 1., e = 20., \omega_1^0 = 0.2.$
$\vartheta_0 = 1.479, \omega_{30} = 0.5652.$
(d) $B_{11}/B_{22} = 0.8, B_{33}/B_{22} = 1.2, p = 3., l = 1., e = 20., \omega_1^0 = 0.2.$
$\vartheta_0 = 2.374, \omega_{30} = 1.725.$

$$\begin{aligned} \xi_1 &= \int_0^s \cos\vartheta\, ds, \\ \xi_2 &= \int_0^s \sin\vartheta \sin\psi\, ds, \\ \xi_3 &= -\int_0^s \sin\vartheta \cos\psi\, ds. \end{aligned} \tag{6}$$

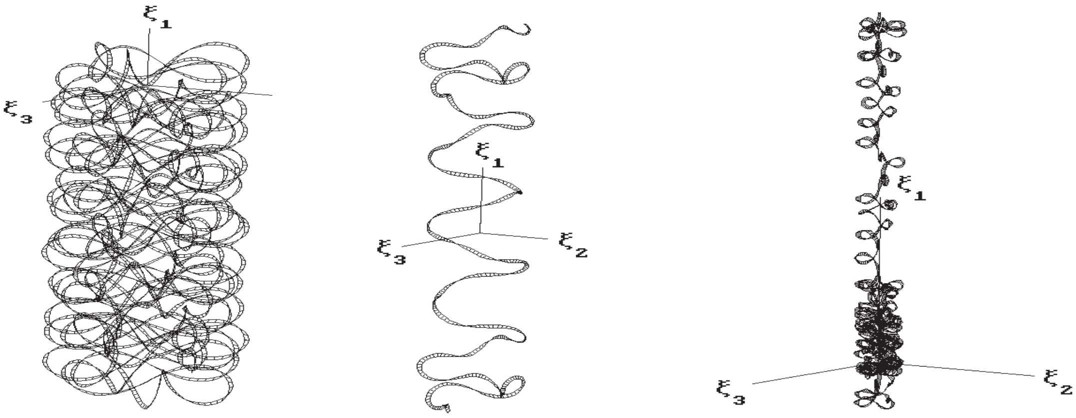


(a) (b) (c)

Figure 4: The shape of the rod in space.

$B_{11}/B_{22} = 0.8, B_{33}/B_{22} = 1.1, p = 5., l = 0., e = 5., \omega_1^0 = 0.2.$

(a) $\vartheta_0 = 2.793, \omega_{30} = 2.558.$

(b) $\vartheta_0 = 2.234, \omega_{30} = -1.462.$

(c) $\vartheta_0 = 0.9076, \omega_{30} = -.2741.$

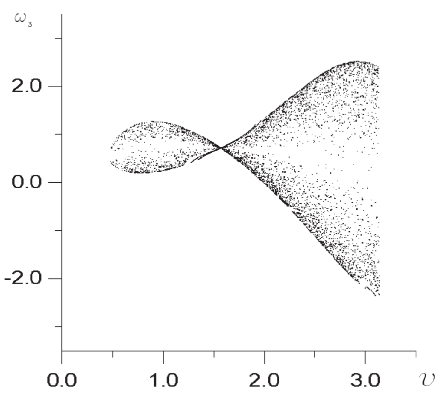


(a)

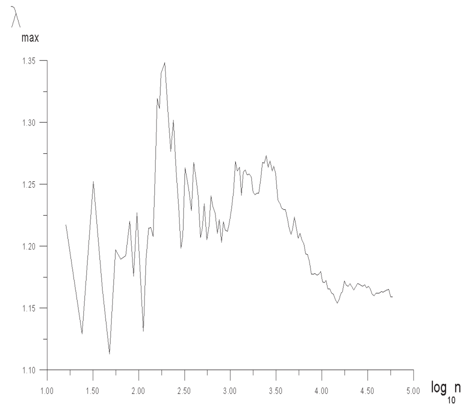


(b)

Figure 5: (a) Poincaré maps of $(\vartheta, \omega_3)$ plane. $\varphi = 2\pi k, k$ integer.
(b) Maximal Lyapunov exponent.
$B_{11}/B_{22} = 0.8, B_{33}/B_{22} = 1.4, p = 4., l = 1., e = 5., \omega_1^0 = 0.2.$